IET Renewable Power Generation

Research Article

Control strategy of switching regulators for fuel-cell power applications

ISSN 1752-1416
Received on 16th August 2016
Revised 28th November 2016
Accepted on 18th January 2017
E-First on 2nd May 2017
doi: 10.1049/iet-rpg.2016.0717
www.ietdl.org

Luis H. Diaz-Saldierna[1,2] ✉, Jesus Leyva-Ramos[1], Diego Langarica-Cordoba[3], Jorge A. Morales-Saldaña[2]

[1]*División de Matemáticas Aplicadas, Instituto Potosino de Investigación Científica y Tecnológica, Camino a la Presa San José No. 2055, CP 78216, San Luis Potosí, México*

[2]*Facultad de Ingeniería, Universidad Autónoma de San Luis Potosí, Zona Universitaria, Av. Dr. Manuel Nava No. 8, CP 78290, San Luis Potosí, México*

[3]*CONACYT-División de Matemáticas Aplicadas, Instituto Potosino de Investigación Científica y Tecnológica, San Luis Potosí, México*

✉ *E-mail: ldiaz@ipicyt.edu.mx*

Abstract: It is often assumed that the input voltage source of a switch-mode power supply is constant or shows negligible small variations. However, the last assumption is no longer valid when a fuel-cell stack is used as input source. A fuel-cell stack is characterised by low and unregulated DC output voltage, in addition, this voltage decreases in a non-linear fashion when the demanded current increases; henceforth, a suitable controller is required to cope the aforementioned issues. In this study, an average current-mode controller is designed using a combined model for a fuel-cell stack and a boost converter; moreover, a selection procedure for the controller gains ensuring system stability and output voltage regulation is developed. The proposed energy system uses a fuel-cell power module (polymer electrolyte membrane fuel cells) and a boost converter delivering a power of 900 W. Experimental results confirm the proposed controller performance for output voltage regulation via closed-loop gain measurements and step load changes. In addition, a comparison between open- and closed-loop measurements is made, where the controller robustness is tested for large load variations and fuel-cell stack output voltage changes as well.

1 Introduction

The integration of renewable and distributed energy generation to the main grid has become an attractive alternative for ancillary services in the last years [1, 2]. For instance, the DC energy sources that perform an important role nowadays are: photovoltaic modules and fuel-cell stacks [3, 4]. These DC sources generate low and unregulated output voltage levels; then, series and parallel arrays are arranged to obtain higher terminal voltage (and current), subsequently power electronic devices are employed to increase, regulate and in some cases invert the output voltage [5, 6].

A fuel cell uses primarily hydrogen as its energy source, which is converted to electrical energy through a complex electrochemical reaction with oxygen or another oxidising agent. In comparison to other energy production sources, this process is more efficient and green, since only heat and water are the waste products; therefore, this technology represents an attractive alternative for power generation [7, 8]. One of the most promising fuel-cell type is the polymer electrolyte membrane fuel cell (PEM fuel cell, also known as proton exchange membrane fuel cell) since it has a relative small size, simple design and low operating temperature, appropriate features for mobile and stationary applications [9, 10]. Additionally to low DC voltage generation, fuel-cell stacks suffer a phenomenon known as *fuel starvation* [11], which refers to an output voltage drop due to fast electric load demand, and directly related to the large time constant (slow dynamics) of the fuel-cell delivery system devices (pumps, valves and in some cases hydrogen reformer).

The DC–DC power converters for fuel-cell applications should have high efficiency, low ripple input current (<10% of nominal fuel-cell stack current) and fast transient response [12]. In power electronics literature, several topologies have been proposed to step up the voltage from fuel-cell stacks, for example: a two-stage cascade converter limiting the current ripple is shown in [13]; a system formed by a fuel-cell stack and a super capacitor, both connected to a boost and buck–boost converters, respectively, is proposed in [14]; a discussion of an electric model for a combined system fuel-cell stack/DC–DC converter is developed in [15] where experimental verification is done in the frequency domain; finally, a three-stage boost converter with a fuel-cell stack as the input source is given in [16]. The operation of fuel-cell-based energy systems in closed loop can be classified as linear and non-linear. From the linear approach, two control schemes are identified: voltage-mode control (VMC) and current-mode control (CMC). In contrast to VMC, CMC strategy has demonstrated a faster transient response, over-current protection and *stronger* stability due to the multiloop nature as well [16].

Research work has been reported using non-linear and advance control in the open literature to operate a fuel-cell-based energy system properly. For instance, the control of a high voltage ratio DC/DC converter coupled to a fuel-cell stack is detailed in [17]. This scheme is based on a dual-loop control that contains a proportional–integral (PI) voltage loop and a fast current loop using a non-linear sliding controller. Additionally, the voltage loop is latter replaced by an energy loop based on a differential flatness control approach. On the other hand, a non-linear single-loop feedback control scheme is proposed in [18, 19] to regulate the operation of a fuel-cell-based energy system. This scheme is based on the differential flatness concept as well, which achieves the desired response using a simple algorithm. Validation of the proposed scheme was achieved by experimental results, where steady-state response, dynamic response and control robustness were verified.

In addition, the controller design for a fuel-cell stack connected to a boost power converter is detailed in [20]. In this work, it is shown that time varying, state feedback controllers, based on integral passive output feedback, semi-globally stabilise the regulation error to zero for a large class of power electronics devices. The performance of the closed-loop system is evaluated through simulation results. Besides, the problem of operating a hybrid energy storage system consisting of a fuel cell and a supercapacitor is treated in [21]. In this case, based on the system non-linear model, a controller is designed making use of

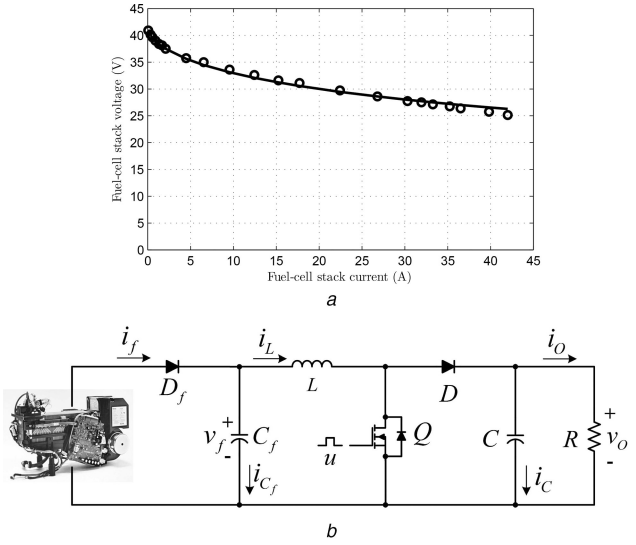

Fig. 1 *Fuel-cell stack/boost converter system*
(a) Nexa power module static output characteristics, data (circles), model (solid line), ***(b)*** Fuel-cell stack/boost converter system

backstepping and Lyapunov stability design techniques. Using both analysis and simulations it is shown that the proposed controller fulfils all control objectives; however, no experimental results are given.

This paper aims to give a general insight over the mechanisms of control when the characteristics of the input source (specifically a fuel-cell stack) are used. Concisely, a PEM fuel-cell stack is connected to a boost converter feeding a resistive load. The main contribution relies on the design of a robust controller to cope properly large step load changes in combination with the associated stack output voltage variations. To this end, first, a combined model is proposed to represent the overall fuel-cell stack/power converter system. Based on this model, two control loops are implemented for voltage regulation. Experimental results of the whole system prove the effectiveness of load voltage regulation under the proposed design approach. Equally important, an easy-to-use selection criteria for the voltage and current control loop gains is developed. In comparison with the work cited above, the proposed low-cost controller is relatively simple, useful, understandable, practical, applicable and scalable.

The paper is organised as follows. The analysis, description and dynamic behaviour of the fuel-cell stack/boost converter system are given in Section 2. In Section 3, a control strategy is proposed together with the tuning parameter selection process. Experimental results to validate the controller performance are shown in Section 4 and finally some concluding remarks are addressed in Section 5.

2 Combined fuel-cell stack/boost converter model

A fuel cell is an hydrogen-based electrical energy source that generates low and unregulated DC voltage, where the output voltage decreases in a non-linear fashion when the demanded current increases. The stack output voltage terminals are connected to a DC/DC power converter to finally provide a voltage required to feed either a DC or a AC load. In the following, an overall mathematical description capturing precisely the coupling between the fuel-cell stack and a DC/DC boost converter is shown in detail.

2.1 Fuel-cell stack static properties

Several expressions have been proposed in the open literature to predict the chemical and thermal dynamical behaviour of PEM fuel cells [22, 23]. However, for the purpose of this work, a suitable and easy-to-handle fuel-cell stack expression including electric properties compatible with power conversion is used. For instance, a fuel-cell stack static expression for the output voltage which depends on the output current and physical parameters is given in [13]

$$v_{\mathrm{f}}(i_{\mathrm{f}}) = \frac{E_{\mathrm{O}}}{1 + (i_{\mathrm{f}}/I_{\mathrm{h}})^{\delta}} \tag{1}$$

where v_{f} is the fuel-cell stack output voltage, i_{f} is the fuel-cell stack current and E_{O} is the open-circuit voltage. The parameters δ and I_{h} depend on the environment humidity conditions and stack temperature. These parameters together with E_{O} are required to be computed for a given fuel-cell stack. A Nexa module is used and characterised in this work. It is a small, low maintenance and fully automated PEM fuel-cell stack, which delivers an output power of 1.2 kW at 24 V voltage. In addition, to avoid reversal current entering to the fuel-cell stack, this module includes a protection diode D_{f}. Unfortunately, this diode yields to an undesired power dissipation, which results in a reduction of usable output power to about 1 kW.

Remark 1: The expression that represents the static properties of the fuel-cell stack (1) was taken from [13]; however, a methodology is required to obtain (from available measured data) the parameters δ and I_{h}.

In the following, an explanation about the computation of the parameters E_{O}, δ and I_{h} is given. A set of N discrete experimental samples $(i_{\mathrm{fexp}}(k), v_{\mathrm{fexp}}(k))$ with $k = 1, 2, 3, \ldots, N$, corresponding to the stack output current and voltage are required. In this case, the samples are depicted in circles in Fig. 1*a*. Observe that such samples are obtained by increasing i_{f} from 0 to 43 A (decreasing a resistive load). Note that there is no load connected to the stack at the very first sample; therefore, the open-circuit voltage is $E_{\mathrm{O}} = v_{\mathrm{fexp}}(1)$ when $i_{\mathrm{fexp}}(1) = 0$ A.

Now, the expression (1) can be rewritten as

$$\left(\frac{i_{\mathrm{f}}}{I_{\mathrm{h}}}\right)^{\delta} = \frac{E_{\mathrm{O}}}{v_{\mathrm{f}}} - 1, \tag{2}$$

and recalling some basic logarithm properties, (2) can be expressed as

$$\delta \log i_{\mathrm{f}} - \delta \log I_{\mathrm{h}} = \log\left(\frac{E_{\mathrm{O}}}{v_{\mathrm{f}}} - 1\right). \tag{3}$$

Assuming that (3) holds for all recorded samples $(i_{\mathrm{fexp}}(k), v_{\mathrm{fexp}}(k))$ with E_{O} known, then (3) has the form

$$a_1 x + a_0 = y, \tag{4}$$

where

$$\begin{aligned} a_1 &= \delta, \\ x &= \log i_{\mathrm{f}}, \\ a_0 &= -\delta \log I_{\mathrm{h}}, \\ y &= \log\left(\frac{E_{\mathrm{O}}}{v_{\mathrm{f}}} - 1\right), \end{aligned} \tag{5}$$

thus, the constants a_1 and a_0 are required to be found in order to compute δ and I_{h}.

Finally, using the well-known linear least square data fitting [24], the parameters δ and I_{h} can be obtained from the following computations (all sums are of the form $\sum_{k=1}^{N}$):

$$\begin{aligned} x_k &= \log(i_{\mathrm{fexp}}(k)), \\ y_k &= \log\left(\frac{E_{\mathrm{O}}}{v_{\mathrm{fexp}}(k)} - 1\right), \\ a_0 &= \frac{\sum x_k^2 \sum y_k - \sum x_k y_k \sum x_k}{N \sum x_k^2 - (\sum x_k)^2}, \end{aligned} \tag{6}$$

which yield to

$$\delta = \frac{N\sum x_k y_k - \sum x_k \sum y_k}{N\sum x_k^2 - (\sum x_k)^2} = 0.64,$$
$$I_{\mathrm{h}} = \log^{-1}\left(-\frac{a_0}{\delta}\right) = 82.86, \tag{7}$$

for $N = 22$ samples and $E_{\mathrm{O}} = 41.7$ V. A comparison between experimental data and the expression in (1) is given in Fig. 1*a*, which confirms the accuracy of the described method. In addition, this static model (1) is continuous for a large range of currents, including no current and maximum current.

2.2 Overall mathematical representation

The proposed physical implementation of the fuel-cell stack/boost converter system is shown in Fig. 1*b*, where Q is the active switch [metal–oxide–semiconductor field-effect transistor (MOSFET)], u the duty cycle, D the diode, L the filter inductor, C the filter capacitor and R the load resistance. Subsequently, i_{f}, i_{Cf}, i_L, i_{C} and i_{O} are the average fuel-cell, coupling capacitor, inductor, capacitor and output currents, respectively. Finally, the average fuel-cell voltage and output (capacitor) voltage are v_{f} and v_{O}, respectively. In this work, it is assumed that the boost converter operates in continuous conduction mode, i.e. the inductor current never decays to zero [25].

The dynamic behaviour of many classes of power circuits are analysed using the notion of average models, which can be manipulated using standard circuit techniques. Average models can be derived for high-frequency switching converters, where linearisation can be easily carried out [26]. In this sense, using Kirchhoff laws when Q is ON/OFF and the current i_{f} from (2), the average (ripple-free) continuous non-linear model is obtained as

$$\begin{aligned}
\dot{v}_{\mathrm{f}} &= \frac{1}{C_{\mathrm{f}}}\left(I_{\mathrm{h}}\left(\frac{E_{\mathrm{O}}}{v_{\mathrm{f}}} - 1\right)^{1/\delta} - i_L\right),\\
\dot{i}_L &= \frac{1}{L}(v_{\mathrm{f}} - (1-u)v_{\mathrm{O}}),\\
\dot{v}_{\mathrm{O}} &= \frac{1}{C}\left((1-u)i_L - \frac{v_{\mathrm{O}}}{R}\right),
\end{aligned} \tag{8}$$

where the state vector is $[v_{\mathrm{f}}, i_L, v_{\mathrm{O}}]^{\mathrm{T}} \in \mathbb{R}_+^3$ and the input $u \in (0\ \ 1)$. The non-linear differential equations in (8) are said to be bilinear, since the input signal u is multiplying the state variables v_{O} and i_L directly. Observe that the restrictions $v_{\mathrm{f}} \in \mathbb{R}_+$ and $i_L \in \mathbb{R}_+$ avoid the indetermination in the first differential equation and ensures the continuous conduction mode operation.

Remark 2: A link capacitor is connected in between the fuel-cell stack and the boost converter, meanwhile [27] uses a series inductor for the same task.

In steady state, the average output voltage V_{O} is greater than the input V_{f}, also the inductor current I_L equals to the fuel-cell current I_{f}; therefore, the nominal operating conditions of (8) are found to be

$$\begin{aligned}
V_{\mathrm{O}} &= \frac{V_{\mathrm{f}}}{1-U},\\
I_L &= \frac{V_{\mathrm{O}}}{R(1-U)} = I_{\mathrm{h}}\left(\frac{E_{\mathrm{O}}}{V_{\mathrm{f}}} - 1\right)^{1/\delta},
\end{aligned} \tag{9}$$

Once the nominal output voltage V_{O} is defined, the resulting fuel-cell voltage V_{f} can be computed from the numerical solution of

$$V_{\mathrm{f}} + \frac{V_{\mathrm{O}}^{2\delta}}{(RI_{\mathrm{h}})^{\delta}} V_{\mathrm{f}}^{1-\delta} - E_{\mathrm{O}} = 0. \tag{10}$$

Note that ideal components and zero voltage losses are assumed in (8)–(10); therefore, the numerical results may differ from those in practice. Furthermore, in steady-state CCM operation, the voltage and current ripples for the boost converter due to the switching action can be computed by

$$\Delta V_{\mathrm{O}} = \frac{I_{\mathrm{O}} U}{C f_{\mathrm{s}}}, \quad \Delta I_L = \frac{V_{\mathrm{f}} U}{L f_{\mathrm{s}}}, \tag{11}$$

additionally, to ensure CCM, the inductor value must be selected as

$$L > \frac{U(1-U)^2 R}{2 f_{\mathrm{s}}}. \tag{12}$$

Linearising around the equilibrium point

$$\mathscr{E} := (V_{\mathrm{f}}, I_L, V_{\mathrm{O}}) \in \mathbb{R}_+^3, \tag{13}$$

yields to the linear average small-signal model for the overall system as

$$\begin{bmatrix} \dot{\tilde{v}}_{\mathrm{f}} \\ \dot{\tilde{i}}_L \\ \dot{\tilde{v}}_{\mathrm{O}} \end{bmatrix} = \begin{bmatrix} -\frac{1}{C_{\mathrm{f}}\kappa} & -\frac{1}{C_{\mathrm{f}}} & 0 \\ \frac{1}{L} & 0 & -\frac{1-U}{L} \\ 0 & \frac{1-U}{C} & -\frac{1}{RC} \end{bmatrix} \begin{bmatrix} \tilde{v}_{\mathrm{f}} \\ \tilde{i}_L \\ \tilde{v}_{\mathrm{O}} \end{bmatrix} + \begin{bmatrix} 0 \\ \frac{V_{\mathrm{O}}}{L} \\ -\frac{I_L}{C} \end{bmatrix} \tilde{u} \tag{14}$$

where the new state vector is $[\tilde{v}_{\mathrm{f}}, \tilde{i}_L, \tilde{v}_{\mathrm{O}}]^{\mathrm{T}} \in \mathbb{R}^3$ and

$$\kappa = \frac{E_{\mathrm{O}} \delta I_{\mathrm{h}}^{\delta} I_{\mathrm{f}}^{\delta-1}}{(I_{\mathrm{h}}^{\delta} + I_{\mathrm{f}}^{\delta})^2}. \tag{15}$$

The resulting model (14) combines two subsystems dynamics and has only one input $\tilde{u} \in \mathbb{R}$. This linear time-invariant model describes approximately the behaviour of the fuel-cell stack/boost converter system for frequencies up to half of the switching frequency f_{s}. Furthermore, it can be used for analysis and controller design of switching regulators.

3 Average current-mode controller

Average CMC is a useful technique for easing the design and improving the dynamic performance of switch-mode converters. Here, a methodology to properly select the controller gains for stability and performance purposes is provided. Since the average inductor current is used for output voltage regulation, a faster response is obtained when step changes are applied to the load. Additionally, sensing the inductor current can also be used for preventing overload current through the converter. This control technique uses a high-gain compensator, a low-pass filter and a PI controller to warrant: (i) that the average inductor current follows the current reference, and (ii) output voltage regulation. The advantage of this approach is that any change in the input voltage source has an immediate effect in the controller (fast propagation property).

The overall controller design procedure is a twofold problem: (i) gain selection for the current loop, and (ii) gain selection for the voltage loop. In order to derive the controller expressions, a configuration for this technique is proposed in Fig. 2. As can be seen, the average CMC employs current and voltage loops. For the current loop, N is the current sensor gain, $G(s)$ a high-gain compensator, $F(s)$ a low-pass filter and finally V_{P} the peak magnitude of the ramp used to generate the control pulses. For the voltage loop, H stands for the voltage sensor gain, V_{ref} the desired output voltage and $K(s)$ the transfer function corresponding to the PI controller, which generates the current reference I_{ref}.

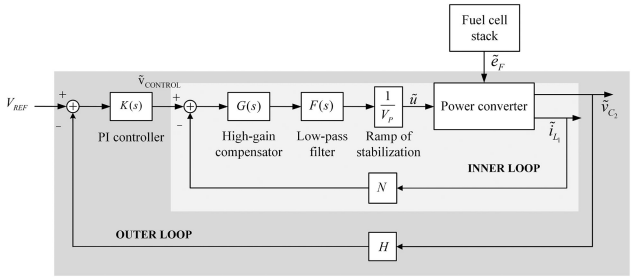

Fig. 2 *Average CMC scheme for a switching regulator*

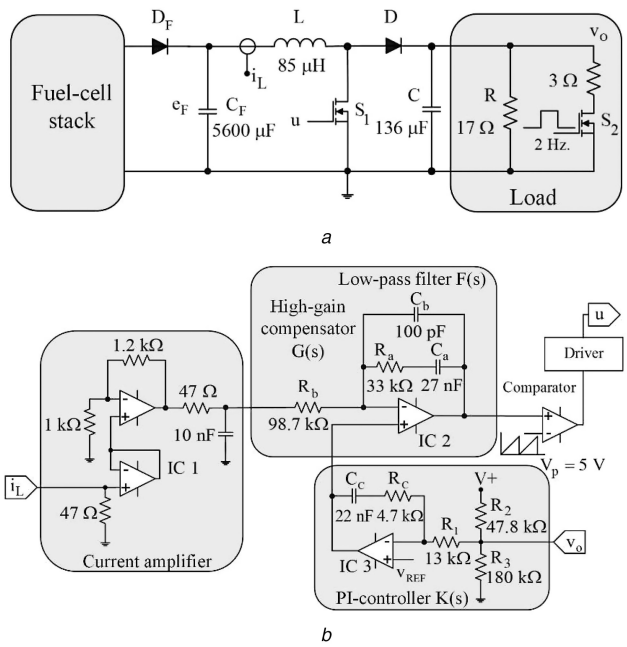

Fig. 3 *Switching regulator*
(a) Combined fuel-cell stack/boost converter, ***(b)*** Average current-mode controller

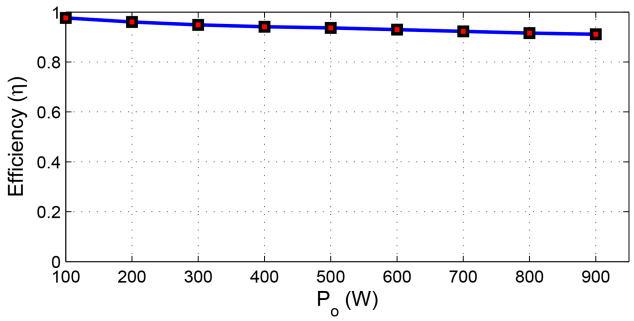

Fig. 4 *Experimental efficiency (η) of the power converter. Efficiency ranges from 97.6% (100 W) to 91.1% (900 W)*

Remark 3: The control scheme proposed in [28] has two control loops for output voltage regulation as well, but the high-gain compensator and the low-pass filter are integrated to the voltage loop, meanwhile the current loop is implemented by a hysteresis controller.

For robust stability of each loop, the following requirements have to be satisfied:

i. for relative stability, the slope at or near cross-over frequency must be not more than −20 dB/dec;
ii. to improve steady-state accuracy, the gain at low frequencies should be high;
iii. for robust stability, appropriate gain and phase margins are required.

In the following, easy-to-use formulae are given to ensure appropriate loop gains characteristics of the closed loops. The poles and zeros for the proposed controller are set mainly from the operating switching frequency of the converter.

3.1 Current loop

The control law $\tilde{u}$ is defined by

$$\tilde{u} = \frac{1}{V_P}\underbrace{\left(\frac{1}{1+(s/\omega_P)}\right)}_{F(s)}\underbrace{\left(G_P\frac{((s/\omega_Z)+1)}{s/\omega_Z}\right)}_{G(s)}(I_{ref}-Ni_L), \tag{16}$$

where ω_P stands for the location of the filter pole, G_P is the compensator gain, ω_Z is the location of the compensator zero and I_{ref} is the output of the voltage loop. Note that both transfer functions $F(s)$ and $G(s)$ can be implemented using a single operational amplifier as shown in Fig. 3. The criteria to select the controller gains (circuit components) are performed following the procedure given below:

- The zero ω_Z of the high-gain compensator should be placed at least a decade below of half of the PWM switching frequency, $f_s/2$. Practically, the zero is determined by the relationship

$$\omega_Z = \frac{1}{R_aC_a}, \tag{17}$$

  where R_a and C_a are the resistance and capacitance corresponding to the current loop control circuit.
- The pole ω_P of the low-pass filter, on the other hand, should be placed either at $f_s/2$ or above. Using the circuitry in Fig. 4, the pole is determined by

$$\omega_P = \frac{C_a+C_b}{R_aC_aC_b}, \tag{18}$$

  where C_b is the capacitor associated to the current loop circuit as well.
- The compensator gain is computed by

$$G_P = \frac{R_a}{R_b}, \tag{19}$$

  where the resistance values must be carefully selected such that

$$G_P < \frac{5(1-U)^2R}{NV_O}. \tag{20}$$

3.2 Voltage loop

The outer loop should be designed to provide a suitable steady-state correction of the output voltage and can be implemented using a PI controller. The output of this loop is the current reference

$$I_{ref} = \underbrace{K_C(1+(1/T_is))}_{K(s)}(V_{ref}-Hv_O), \tag{21}$$

where K_C is the proportional gain, T_i is the integral time and V_{ref} is the reference output voltage.

In this case, the selection criteria should follow:

- The proportional gain $K_P = R_C/R_i$ is selected such that

$$K_P < \frac{10(1-U)}{HV_O}, \tag{22}$$

  where the voltage divider is

$$H = \frac{R_1 \| R_3}{R_1 \| R_3 + R_2}. \tag{23}$$

- Finally, the integral time is computed from

$$T_i = R_C C_C, \tag{24}$$

where R_C and C_C are the resistance and capacitance values of the PI controller circuit, which must be selected such that $1/T_i$ is placed at least one decade below f_s.

Table 1 Boost converter components

capacitor C_f	5600 μF
capacitor C	136 μF
inductor L	85 μH
nominal load R	2.56 Ω
diode D	80EVU02
MOSFET S_1	IRFP4568 × 2
MOSFET S_2	IRF740 × 2
modulator	LM311

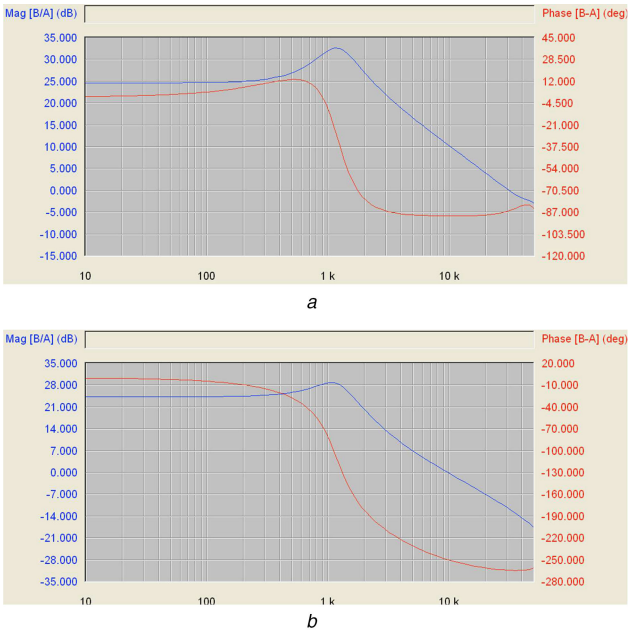

Fig. 5 *Experimental frequency response for a 2.56 Ω load*
(a) Transfer function $\tilde{i}_L/\tilde{u}$. (Top) magnitude (5 dB/div), and (bottom) phase (16.5°/div), ***(b)*** Transfer function $\tilde{v}_O/\tilde{u}$. (Top) phase (30°/div) and (bottom) magnitude (7 dB/div), (*x*-axis in Hz)

Remark 4: In contrast to VMC, here an inner loop is added. This improves significantly the transient performance of the controller, since the transfer function $\tilde{v}_O/\tilde{u}$ of a boost converter has a right half-plane zero, and a single voltage loop may not deal properly with this issue.

4 Experimental results

A fuel-cell stack/boost converter and the corresponding controller (16) have been implemented in the laboratory as shown Fig. 4. The converter parameters are given in Table 1. The inductor current is measured via the transducer LA50-P by LEM, which results in the sensor gain $N = 0.071$. The Nexa Power Module delivers an output voltage V_f, ranging from 22 to 42 V. The boost converter nominal duty cycle U is set to 0.56, providing an output voltage of $V_O = 48$ V, feeding a nominal resistive load of $R = 2.56$ Ω. The total output power is around 900 W, which requires an averaged fuel consumption of 12.2 standard litre per minute.

Furthermore, the switching frequency is set to 100 kHz. The peak magnitude of the ramp V_P is 5 V and the voltage sensor gain H is 0.20. The parameters of the controller are selected following the above criteria: $f_Z = \omega_Z/2\pi = 178.62$ Hz, $G_P = 0.33$, $f_P = \omega_P/2\pi = 48.4$ kHz, $K_P = 0.36$ and $T_i = 0.103$ ms. Open- and closed-loop experimental tests were performed considering step changes in the load resistance through the switch S_2. These variations range from 2.56 to 17 Ω; that is from full to 10% of load at a frequency of 2 Hz.

The converter efficiency ($\eta = P_o/P_i$, where P_o is the output power and P_i is the input power of the converter) is shown in Fig. 4, as can be seen, the efficiency reduces when the output power is increased.

4.1 Open-loop test

The experimental response of the transfer function $\tilde{i}_L/\tilde{u}$ is shown in Fig. 5*a*, while the experimental response of the transfer function $\tilde{v}_O/\tilde{u}$ is shown in Fig. 5*b*. These transfer functions were measured at nominal load using the *Frequency Response Analyser 300* from AP Instruments, Inc. Both frequency responses were obtained in open loop, additionally, it is clear from the plots that resonant peaks occur around 1.1 kHz.

The experimental open-loop time response of the system is shown in Fig. 6*a*. It is noticeable that the experimental results are close enough to the theoretical relation given in (9). Using the MOSFET S_2 (trigger voltage V_g), step changes of 2 Hz are applied to the output load which ranges from 2.56 to 17 Ω. The resulting output voltage V_O is shown in Fig. 6*b*, which changes for about 33 V. On the other hand, Fig. 6*c* shows the step changes on the fuel-cell side. As can be seen, the fuel-cell stack output voltage ranges from 23 to 33 V and the demanded current changes from about 9 to 30 A.

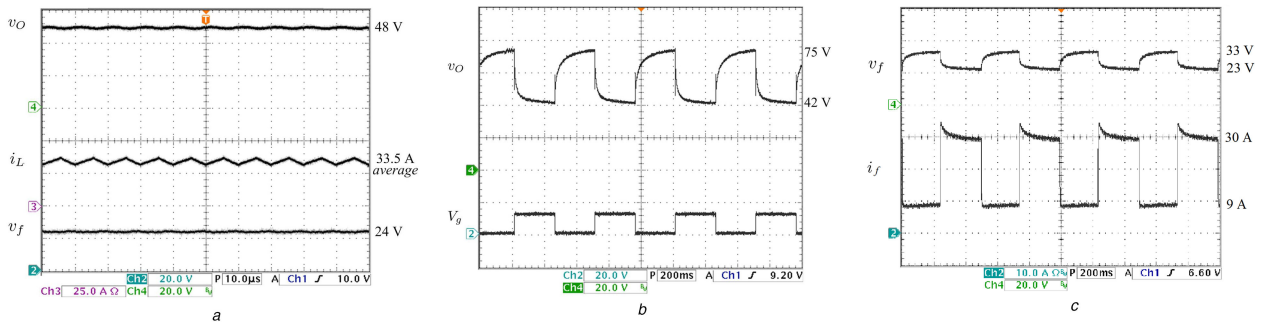

Fig. 6 *Experimental results in open-loop response for step changes in the load between 2.56 and 17 Ω*
(a) (From top to bottom) output voltage v_O (20 V/div), inductor current i_L (25 A/div) and fuel-cell voltage v_f (20 V/div) (time: 10 μs/div), ***(b)*** (From top to bottom) output voltage v_O (20 V/div) and gate voltage V_g of MOSFET S_2 (20 V/div) (time: 200 ms/div), ***(c)*** (From top to bottom) output voltage of the fuel-cell stack v_f (20 V/div) and output current of the fuel-cell stack i_f (10 A/div) (time: 200 ms/div)

4.2 Closed-loop test

The experimental frequency response of the loop gain $L(s)$, i.e. the product of the transfer functions around the voltage loop, at nominal load is shown in Fig. 7. The magnitude plot exhibits a high gain at low frequencies, additionally, the controller provides a 8 kHz crossover frequency, concluding that the loop gain has sufficient gain and phase margins; therefore, the switching regulator is robust to parameter variations.

The switching regulator operating condition corresponding to 48 V output voltage at nominal load (no load changes) is shown in Fig. 8*a*. At this operating condition, the fuel-cell stack is delivering a voltage of 24 V. When output load changes are introduced, the resulting load voltage remains at 48 V as shown in Fig. 8*b*, where it is clear the switching regulator is robust under large load variations. As consequence of these changes, the fuel-cell stack voltage changes between 26 and 38 V. The demanded current ranges from 4 to 27 A, as is shown in Fig. 8*c*. There are significant differences between current and voltage levels in Figs. 6*c* and 8*c*, respectively. This is due to the stored energy in the capacitor C_F that helps to compensate the changes in the demanded energy for closed-loop response. Note that the fuel-cell current in the open-loop case (Fig. 6*c*) presents a 5 A overshoot, meanwhile in the closed-loop case (Fig. 8*c*), the current does not present any overshoot; therefore, the life cycle of the fuel cell is not overwhelmed. The current ripple is shown in Fig. 8*d*, which is small (1.2 A peak to peak) due to the capacitor C_F.

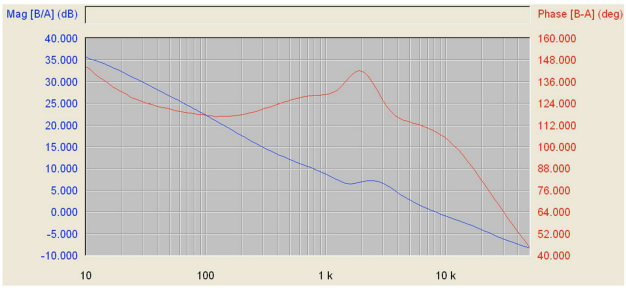

Fig. 7 *Experimental frequency response of the loop gain L(s) for a 2.56 Ω load. (Bottom) magnitude (5 dB/div) and (top) phase margin (18°/div), x-axis in Hz*

5 Conclusions

This paper deals with the output voltage regulation of a fuel-cell stack/boost converter system. The proposed control strategy is based on average CMC where two loops are implemented, namely the inner loop where the inductor current is fed back using a high-gain compensator and a low-pass filter, and the outer loop where the output voltage is fed back via a PI controller for steady-state error regulation. The selection procedure for the controller parameters is explicitly detailed. The criteria given within ensure system stability and output voltage regulation. The poles and zeros for the controller are set mainly from the operating switching frequency of the converter. Additionally, due to the high-gain compensator of the inner loop, the converter performance is less sensitive to parameter uncertainties and variations of the fuel-cell stack voltage. This control strategy was implemented using low-cost operational amplifiers, suitable for commercial applications. Finally, experimental results using a 900 W boost converter prototype show good robustness to large variations on the load.

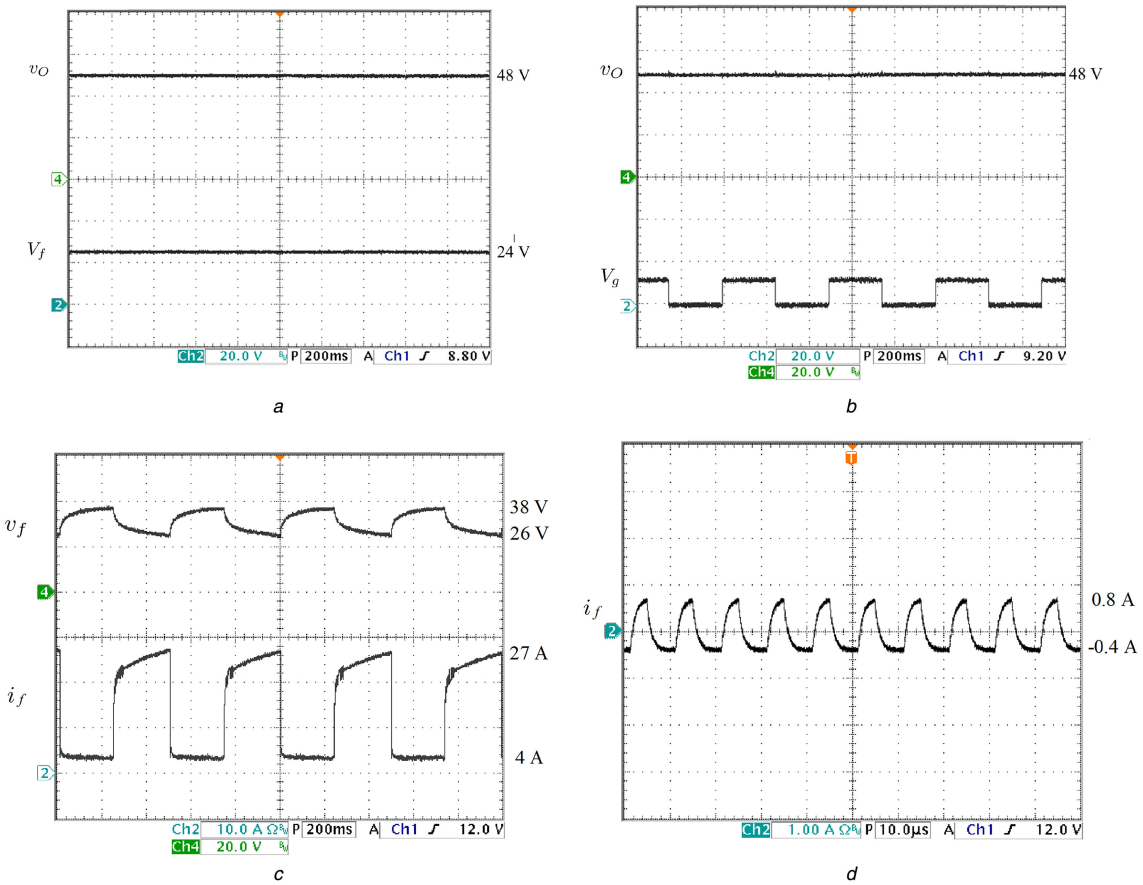

Fig. 8 *Closed-loop response*

(a) Response at nominal load (2.56 Ω). (From top to bottom) output voltage v_O (20 V/div) and fuel-cell voltage v_f (20 V/div) (time: 200 ms/div), ***(b)*** Response to step changes in the load between 2.56 and 17 Ω: (from top to bottom) output voltage v_O (20 V/div) and gate voltage V_g of MOSFET S_2 (20 V/div) (time: 200 ms/div), ***(c)*** Response to step changes in the load between 2.56 and 17 Ω: (from top to bottom) fuel-cell voltage v_f (20 V/div), and output current of the fuel-cell stack i_f (10 A/div) (time: 200 ms/div), ***(d)*** Output current ripple of the fuel-cell stack i_f (1 A/div) (time: 10 µs/div)

6 References

[1] Carrasco, J.M., Garcia, L., Bialasiewiez, J.T., *et al.*: 'Power-electronic system for the grid integration of renewable energy sources', *IEEE Trans. Ind. Electron.*, 2006, **53**, (4), pp. 1002–1016

[2] Benson, Ch.L., Magee, Ch.L.: 'On improvement rates for renewable energy technologies: solar PV, wind, capacitors, and batteries', *J. Renew. Energy*, 2014, **68**, pp. 745–751

[3] Shen, J.-M., Joul, H.-L., Wu, J.-C.: 'Transformerless three-port grid-connected power converter for distribution power generation system with dual renewable energy sources', *IET Power Electron.*, 2012, **5**, (1), pp. 501–509

[4] Jakhar, H., Soni, M.S., Gakkhar, N.: 'Historical and recent development of concentrating photovoltaic cooling technologies', *Renew. Sustain. Energy Rev.*, 2016, **60**, pp. 41–59

[5] Bahceci, S., Fedakar, S., Yalcinoz, T.: 'Examination of the grid-connected polymer electrolyte membrane fuel cell's electrical behaviour and control', *IET Renew. Power Gener.*, 2016, **10**, (3), pp. 388–398

[6] Rahmal, S.A., Varmal, R.K., Vanderheide, T.: 'Generalised model of a photovoltaic panel', *IET Renew. Power Gener.*, 2014, **8**, (3), pp. 217–229

[7] Li, Q., Chen, W., Liu, Z., *et al.*: 'Active control strategy based on vector proportion integration controller for proton exchange membrane fuel cell grid-connected system', *IET Renew. Power Gener.*, 2015, **9**, (8), pp. 991–999

[8] Thounthong, P., Davat, B., Rael, S., *et al.*: 'Fuel cell high-power applications', *IEEE Ind. Electron. Mag.*, 2009, **3**, pp. 32–46

[9] Kabalo, M., Pairel, D., Blunier, B., *et al.*: 'Experimental evaluation of four-phase floating interleaved boost converter design and control for fuel cell applications', *IET Power Electron.*, 2013, **6**, (2), pp. 215–226

[10] Leel, J.-G., Choe, S.-Y., Ahn, J.-W., *et al.*: 'Modelling and simulation of a polymer electrolyte membrane fuel cell system with a PWM dc/dc converter for stationary applications', *IET Power Electron.*, 2008, **1**, (3), pp. 305–317

[11] Thounthong, P., Davat, B.: 'Study of a multi-phase interleaved step-up converter for fuel cell applications', *Energy Convers. Manage.*, 2010, **51**, pp. 826–832

[12] Naik, M.V., Samuel, P.: 'Analysis of ripple current, power losses and high efficiency of dc–dc converters for fuel cell power generating systems', *Renew. Sustain. Energy Rev.*, 2016, **59**, pp. 1080–1088

[13] Shahin, A., Hinaje, M., Martin, J.-P., *et al.*: 'High voltage ratio dc–dc converter for fuel-cell applications', *IEEE Trans. Ind. Electron.*, 2010, **57**, (12), pp. 3944–3955

[14] Hajizade, A., Golkar, M.A., Feliachi, A.: 'Voltage control and active power management of hybrid fuel-cell/energy-storage power conversion system under unbalanced voltage sag conditions', *IEEE Trans. Energy Convers.*, 2010, **25**, (4), pp. 1195–1208

[15] Vazquez-Oviedo, E.I., Ortiz-Lopez, M.G., Diaz-Saldierna, L.H., *et al.*: 'Modeling study of a combined fuel-cell stack/switch mode dc–dc converter', *J. Fuel Cell Sci. Technol.*, 2014, **11**, pp. 1–5

[16] Leyva-Ramos, J., Lopez-Cruz, J.M., Ortiz-Lopez, M.G., *et al.*: 'Switching regulator using a high step-up voltage converter for fuel-cell modules', *IET Power Electron.*, 2013, **6**, (8), pp. 1626–1633

[17] Saadi, R., Kraa, O., Ayad, M.-Y., *et al.*: 'Dual loop controllers using PI, sliding mode and flatness controls applied to low voltage converters for fuel cell applications', *Int. J. Hydrog. Energy*, 2016, **41**, (42), pp. 19154–19163

[18] Thammasiriroj, W., Chunkag, V., Phattanasak, M., *et al.*: 'Nonlinear single-loop control of the parallel converters for a fuel cell power source used in {DC} grid applications', *Int. J. Electr. Power Energy Syst.*, 2010, **65**, pp. 41–48

[19] Thounthong, P., Pierfederici, S.: 'A new control law based on the differential flatness principle for multiphase interleaved DC–DC converter', *IEEE Trans. Circuits Syst. II, Express Briefs*, 2010, **57**, (11), pp. 903–907

[20] Sira-Ramírez, H., Oliver-Salazar, M.-A., Leyva-Ramos, J.: 'Voltage regulation of a fuel cell-boost converter system: a proportional integral exact tracking error dynamics passive output feedback control approach'. American Control Conf. (ACC), Montreal, Canada, June 2012, pp. 2153–2158

[21] El Fadil, H., Giri, F., Guerrero, J.-M., *et al.*: 'Modeling and nonlinear control of a fuel cell/supercapacitor hybrid energy storage system for electric vehicles', *IEEE Trans. Veh. Technol.*, 2014, **63**, (7), pp. 3011–3018

[22] Hoogers, G.: '*Fuel cell technology handbook*' (CRC Press, 2003)

[23] Gou, B., Na, W.-K., Diong, B.: '*Fuel cells, modeling, control and applications*' (CRC Press, 2010)

[24] Chapra, S.-C., Canale, R.-P.: '*Numerical methods for engineers*' (McGraw-Hill, 2010)

[25] Guesmi, K., Essounbouli, N., Hamzaoui, A.: 'Systematic design approach of fuzzy PID stabilizer for dc–dc converters', *Energy Convers. Manage.*, 2008, **49**, pp. 2880–2889

[26] Mohan, N., Undeland, T.-M., Robbins, W.-P.: '*Power electronics converters, applications, and design*' (John Wiley & Sons, 2003, 3rd edn.)

[27] Tran, V.-L., Tran, N.-T., Yu, S.-H., *et al.*: 'Design a nonisolated fuel cell boost charger for lithium polymer batteries with a low output ripple', *IEEE Trans. Energy Convers.*, 2015, **30**, (2), pp. 605–614

[28] Shadmand, M.B., Balog, R.S., Abu-Rub, H.: 'Model predictive control of PV sources in a smart dc distribution system: maximum power point tracking and droop control', *IEEE Trans. Energy Convers.*, 2014, **29**, (4), pp. 913–921